Monte Carlo study of the site-percolation model in two and three dimensions

Youjin Deng[1,2] and Henk W. J. Blöte[2,3]

[1]*Laboratory of Material Science, Delft University of Technology, Rotterdamseweg 137, 2628 AL Delft, The Netherlands*
[2]*Faculty of Applied Sciences, Delft University of Technology, P. O. Box 5046, 2600 GA Delft, The Netherlands*
[3]*Lorentz Institute, Leiden University, P. O. Box 9506, 2300 RA Leiden, The Netherlands*

We investigate the site-percolation problem on the square and simple-cubic lattices by means of a Monte Carlo algorithm that in fact simulates systems with size $L^{d-1} \times \infty$, where L specifies the linear system size. This algorithm can be regarded either as an extension of the Hoshen-Kopelman method or as a special case of the transfer-matrix Monte Carlo technique. Various quantities, such as the magnetic correlation function, are sampled in the finite directions of the above geometry. Simulations are arranged such that both bulk and surface quantities can be sampled. On the square lattice, we locate the percolation threshold at $p_c = 0.592\,746\,5(4)$, and determine two universal quantities as $Q_{gbc} = 0.930\,34(1)$ and $Q_{gsc} = 0.793\,72(3)$, which are associated with bulk and surface correlations, respectively. These values agree well with the exact values $2^{-5/48}$ and $2^{-1/3}$, respectively, which follow from conformal invariance. On the simple-cubic lattice, we locate the percolation threshold at $p_c = 0.311\,607\,7(4)$. We further determine the bulk thermal and magnetic exponents as $y_t = 1.1437(6)$ and $y_h = 2.5219(2)$, respectively, and the surface magnetic exponent at the ordinary phase transition as $y_{hs}^{(o)} = 1.0248(3)$.

PACS number(s): 05.50.+q, 64.60.Cn, 64.60.Fr, 75.10.Hk

I. INTRODUCTION

Percolation problems have been of great research interest to physicists and mathematicians [1], and a variety of applications have been reported [2]. It was determined [3] that the word "percolation" has appeared in the title of almost 4000 physics papers in the last quarter of the past century. In the field of critical phenomena, the percolation theory provides a simple picture and a fascinating illustration of many important concepts in terms of geometric properties. This is mainly due to the Kasteleyn-Fortuin mapping [4], which exactly relates the bond-percolation model and the random-cluster representation of the q-state Potts model [5] in the $q \to 1$ limit. For a review of the Potts model, see Ref. [6]. Thus, a generalized set of percolation models, which are "correlated" and belong to an infinite range of universality classes, is obtained, and rich critical phenomena are observed [7].

The Kasteleyn-Fortuin mapping [4] enables the direct application of much of the knowledge that has been gathered for the Potts model to the percolation model. In particular, owing to exact mappings, Coulomb gas theory, and conformal field theory [7–11], the bulk critical exponents in two dimensions are exactly available: the thermal exponent is $y_t = 3/4$, and the magnetic ones are $y_{h1} = 91/48$ and $y_{h2} = 19/48$ [12], respectively. For the percolation model on the semi-infinite plane with a free surface–i.e., a free one-dimensional edge, the surface magnetic exponent is also exactly known [13] as $y_{hs}^{(o)} = 2/3$, where the superscript (o) represents the "ordinary" surface phase transition.

The upper critical dimensionality of the percolation model is 6 [14], so that universal properties of the percolation model for $d \geq 6$ are expected to be mean-field-like, apart from the possible existence of logarithmic corrections. The mean-field values of thermal and magnetic exponents are $\tilde{y}_t = y_t/d = 1/3$ and $\tilde{y}_h = y_h/d = 2/3$, respectively. For percolation models in $2 < d < 6$ dimensions, however, no exact values are available for y_t and y_h. Therefore, investigations have to depend on various types of approximations, such as series expansions and Monte Carlo simulations.

In comparison with many simulations in statistical physics, such as the Swendsen-Wang algorithm [15] for the Potts model, Monte Carlo studies of the percolation problem are relatively simple. No Markov process is needed to perform importance sampling, and thus no critical slowing down exists. For clarity, we consider the bond-percolation model on a regular lattice. For each pair of nearest-neighbor sites, a uniformly distributed random number $0 \leq r \leq 1$ is produced, and the bond in between is occupied for $r \leq p$ or empty for $r > p$, respectively, where p is the bond-occupation probability. Two sites connected through a chain of occupied bonds are said to percolate, i.e., to be in the same cluster. As a result, the whole lattice is decomposed into a number of clusters, usually including single-site ones. Then, various questions can be asked concerning the distribution of cluster sizes, the fractal dimension of the clusters, the percolation probability, etc.

An extension of the above standard method is the well-known Hoshen-Kopelman [16] algorithm. In this algorithm, the so-called cluster multiple labeling technique is applied, and thus only the state of parts of the lattice sites needs to be stored. Another approach of cluster generation is the Leath method [17]. By means of these algorithms, systems of considerable sizes have been simulated [18,19]. Recently, Newman and Ziff introduced [3] an efficient Monte Carlo algorithm, which allows one to calculate quantities of interest over the entire range of site or bond occupation probabilities from zero to one in a single run. Other numerical methods [20,21] have been developed to answer specific questions about percolation models, such as the hull-generation algorithm.

Naturally, these Monte Carlo simulations are performed for systems of finite extent. In the study of bulk critical behavior, one usually chooses the torus geometry, i.e., a d-dimensional hypercube with periodic boundary conditions in each of the d directions.

Another important numerical method in the study of critical phenomena is the transfer-matrix technique. In contrast to the above Monte Carlo methods, this technique usually applies to systems in a pseudo-one-dimensional geometry, namely $L^{d-1} \times \infty$, with L the side length of the $(d-1)$-dimensional hypercube. In two dimensions, this geometry reduces to the surface of an infinitely long cylinder. The main idea of the transfer-matrix technique is to calculate the partition sum and other quantities by means of matrix operations. Typically, only a few of the leading eigenvalues and the associated eigenvectors are calculated. Various correlation lengths are determined by these eigenvalues. Moreover, in two dimensions, these correlation lengths are exactly related to critical exponents by means of a conformal mapping [22]. The main ingredients of the numerical transfer-matrix method include the construction of the matrix and the repeated multiplication of a state vector by this matrix. The calculations do not involve approximations except for the finite numerical precision of floating-point operations, and thus the numerical uncertainty is only limited to the machine precision, at least in principle. This is in contrast to the aforementioned Monte Carlo simulations, where the dominant errors are usually of a statistical nature, so that the number of samples quadratically increases as a function of the inverse of the required precision. On the other hand, the dimension of the transfer matrix, i.e., the number of elements, increases exponentially as $\propto a^{L^{d-1}}$, where a is a constant. Some additional techniques can be utilized to reduce the requirement of computer memory, such as symmetry operations and the sparse-matrix technique [23,24]. Nevertheless, the maximum system sizes that can be investigated by the sparse transfer-matrix method are rather limited, even with the help of modern computers. In two dimensions, the maximum size L is of order 20, while L in three dimensions is normally restricted to be less than 6. Thus, for $d > 2$, transfer-matrix calculations become less practical.

The size restrictions are alleviated by the transfer-matrix Monte Carlo method, which involves a stochastic representation of the multiplication of the state vector by the transfer matrix. This method is related to the diffusion quantum Monte Carlo method and typically uses a population of random walkers such as described, e.g., in Ref. [25]. The transfer-matrix Monte Carlo method has already been applied to several three-dimensional systems, such as the Ising, XY, and Heisenberg models [26].

Another approach of transfer-matrix Monte Carlo calculations to percolation problems was pioneered by Derrida and Vannimenus [27]. Thus far, it was mainly used to compute the conductivity of random resistor networks [28–31]. In this approach, such a network in geometry $L^{d-1} \times \infty$ is constructed by adding resistors layer by layer (column by column in two dimensions) along the infinite direction. A set of potentials U_i $(i=1,2,\ldots,L^{d-1})$ is then imposed on each site of the newly added layer—i.e., the free surface—and the

currents I_i are measured. In terms of vectors and matrices, the relation between the potentials and the currents can be written as $I=AU$, where A is a random $L^{d-1} \times L^{d-1}$ matrix.

In the present paper, we construct a Monte Carlo method that simulates the percolation model in an $L^{d-1} \times \infty$ geometry. This geometry is obtained by iteratively adding an L^{d-1} layer of lattice sites during each Monte Carlo step. Only the connectivity of the newly added layer is stored in computer memory. Thus, one actually simulates in $(d-1)$ dimensions for d-dimensional percolation models.

The organization of the present paper is as follows. Section II describes the detailed formulation of our algorithm. In Sec. III, the algorithm is applied to the site-percolation model on the square and simple-cubic lattices; the numerical data are analyzed by finite-size scaling. A brief discussion is then given in Sec. IV.

II. ALGORITHM

This section describes the Monte Carlo algorithm used in this work in the language of the site-percolation model on a square lattice of size $L \times \infty$; the infinite-size direction is referred to as the transfer direction t. The lattice sites are denoted by coordinates (t,k) with $1 \leq k \leq L$. For simplicity, we first apply free boundary conditions in the perpendicular direction, i.e., site $(t, 1)$ is not a nearest-neighbor site of (t,L) for $L > 2$. In this case, the geometry $L \times \infty$ reduces to a strip.

Each site is occupied with probability $0 \leq p \leq 1$, and empty with probability $1-p$. Two sites connected through a chain of occupied nearest-neighboring sites are said to be in the same cluster. Each site (t,k) is labeled by a non-negative integer $m_{t,k}$: $m_{t,k}=0$ represents an empty site, while $m_{t,k}>0$ denotes a cluster label. This site labeling is done such that sites in the same cluster are labeled by the same number $m > 0$, while two sites that are not connected are labeled by different numbers $m_{t,k} \neq m_{t,l}$. This information may be called "connectivity" and can be used to construct a transfer matrix for the random-cluster representation of the Potts model [25]. The connectivity on the tth layer is exclusively determined by the first t layers and thus does not change when new layers are added.

The connectivity of layer t, together with the distribution of occupied and empty sites in a newly added layer $t+1$, determines the connectivity of the $(t+1)$th layer. The first version of our algorithm is then formulated as follows.

1. Add a new layer $t+1$ and extend existing clusters to layer $t+1$. For each site $(t+1,k)$ in the $(t+1)$th layer, a uniformly distributed random numbers r_k is drawn to determine whether it is occupied or empty. If site $(t+1,k)$ is occupied and further its nearest-neighbor site in the tth layer is also occupied, i.e., they are connected, one simply sets $m_{t+1,k}=m_{t,k}$. Otherwise, the label $m_{t+1,k}$ remains to be determined. After all sites in layer $t+1$ are visited, the information about the connectivity of the tth layer has no further use, and the corresponding memory is freed.

2. Grow and merge existing clusters in layer $t+1$. Sequentially visit the lattice sites that are labeled in step 1, and form complete clusters for them, as in the conventional Monte Carlo method [16,17]. If two sites $(t+1,k)$ and $(t$
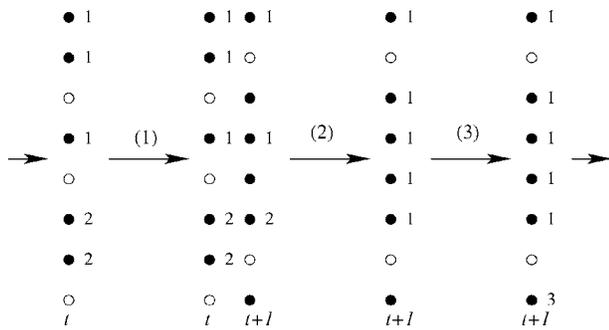
FIG. 1. Illustration of the cluster construction for the newly added layer without the help of the "linkage" technique. This example applies to linear size $L=8$, and free boundary conditions are imposed in the vertical direction.

FIG. 2. Illustration of the cluster construction for the newly added layer with the help of the "linkage" technique. This example applies to linear size $L=8$, and free boundary conditions are imposed in the vertical direction.

$+1,l$) with different cluster labels are connected through a chain of occupied sites, the pertinent clusters are merged, i.e., all sites $(t+1,i)$ with $m_{t+1,l}$ are relabeled as $m_{t+1,i} \leftarrow m_{t+1,k}$.

3. Create new clusters. Clusters are also formed for the remaining occupied sites $(t+1,k)$ that have not been labeled after steps 1 and 2. New cluster labels m are used by increasing the largest existing cluster label by 1.

These steps are shown in Fig. 1. By repeating steps 1–3, an arbitrarily long strip is obtained. This procedure does not keep track of the connectivity along the transfer direction; sampling procedures are performed only on the newly added surface layers.

A. Linkage technique

Among the above steps 1–3, the most time-consuming one is step 2, because a scan of the whole $(t+1)$th layer is required whenever two clusters m and m' merge. This is especially expensive for large system sizes, because the total number of clusters is proportional to the volume of the system. Thus, one expects that the computer time for step 2 increases as $\propto L^{2d-2}$. To improve the efficiency, we introduce a linkage technique.

In addition to the above cluster labeling method, we also link all sites (t,k) in layer t in the same cluster by a "chain" with two open ends (this chain is a two-dimensional array during programming). Further, we construct this linkage in increasing order $k_1 < k_2 < \cdots < k_i < \cdots$ of the in-layer coordinate. Therefore, in the case in which the sites in cluster m are going to be relabeled, one need not scan over the whole layer but just follow the linkage to reach all the lattice sites in this cluster. More specifically, except for the empty sites and those sites at the ends of a chain, each site "points" to two other sites in the same cluster, whose coordinates are closest to that of this site. Both the linkage technique and the cluster-labeling method are independently sufficient to represent a connectivity.

With the linkages of the sites in layer t, the formal version of the algorithm reads as follows.

1. Distribution of the occupied and empty sites in the $(t+1)$th layer.
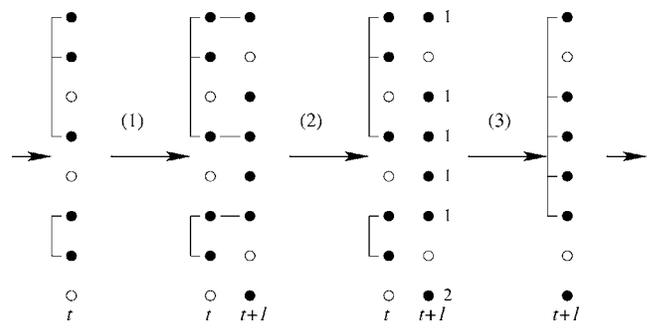
2. Cluster construction using the cluster-labeling method.

Since the connectivity of the tth layer is already completely specified by the linkages, we do not need the previous labels and we set the cluster label m of the first occupied site k as $m_k=1$. The growth of cluster m_k then involves the following two parts. First, visit the nearest-neighbor sites in layer $t+1$. If they are occupied, include them in the cluster labeled by m_k and store their coordinates in a "stack" memory. Second, visit the nearest-neighbor site in layer t. If it is occupied, follow its linkage and visit all sites (t,i) on this linkage. If the corresponding site $(t+1,i)$ in the $(t+1)$th layer is occupied, include it in cluster m_k and store in the "stack." Read a site from the "stack" (and erase it from the "stack"), and repeat the above procedures until cluster m_k is completed. Then, go to the next occupied site in the $(t+1)$th layer that has not yet been labeled, set its label to the next integer m_k+1, and grow a new cluster. Repeat this until all the occupied sites in the $(t+1)$th layer are visited. We mention that, in order to avoid duplicate usages of the linking information of the tth layer, the link between any two sites is immediately deleted after it is used.

3. Linkage creation. After step 2, the connectivity of the new layer is completely specified by cluster labels m. The task of the present step is to derive on the basis of these labels the linking information of the $(t+1)$th layer. First, an additional array is introduced containing a value $l_f(m)$ for each value of the labels m. Its elements are initially set as 0 during step 2. Then, one sequentially visits the occupied sites in layer $t+1$. Suppose the present site is k. Let site $k+1$ be the site that is visited. If site $k+1$ is also occupied, link sites k and $k+1$ to each other; if site $k+1$ is empty, one sets $l_f(m_k)=k$. This means that site k is the last site in the cluster labeled by m_k among sites $1 \leqslant i \leqslant k+1$. In the case that site $k-1$ is empty, one reads the element $l_f(m_k)$. If $l_f(m_k)$ is nonzero, link sites $l_f(m_k)$ and k; otherwise, do nothing. Note that no action is needed if site $k-1$ is occupied, because the link between sites $k-1$ and k was already defined when site $k-1$ was visited.

Iterating steps 1–3 eventually yields a strip $L \times \infty$. The above steps are illustrated in Fig. 2.

Each of the above three steps consists of a number of operations of order L^{d-1}. In comparison with the previous procedure without the linkage technique, the efficiency is improved by a factor of order L^{d-1}.
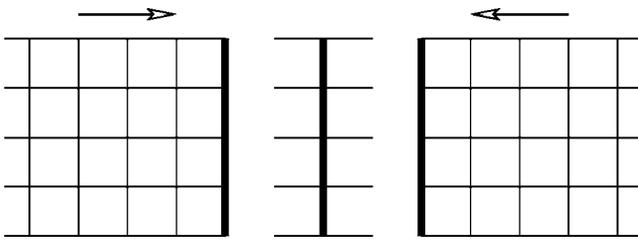
FIG. 3. Illustration of the sampling of bulk quantities. The thick solid lines represent the two free surfaces of the simulated strips and a newly inserted layer of randomly distributed occupied and empty sites, respectively. These layers are "glued" together by adding horizontal bonds.

B. Combined samplings of bulk and surface quantities

During the above procedures, quantities of interest, such as moments of the cluster-size distribution and the correlation functions, can be sampled on each newly added layer. However, this layer is actually the free surface at the end of the strip, and thus does not provide adequate information concerning bulk critical phenomena.

Nevertheless, the procedure can be adapted such that some bulk quantities can be sampled. Instead of a single strip, one simultaneously simulates two independent strips with the same site-occupation probability p. After adding a new layer to each strip, these two new layers are "glued" together by nearest-neighbor bonds. The result is that the connectivity of each of the two layers represents a bulk layer of the percolation model.

In the present work, we slightly modified this procedure by inserting a third layer of randomly occupied and empty lattice sites, also using probability p. Both free surfaces are then connected to the third layer, and bulk quantities are sampled on it. This is illustrated by Fig. 3. In this way, the information about the connectivity of the two free layers, which is still needed for further growing of the strips, is more easily preserved.

C. Generalization

It is straightforward to generalize the above procedures to the bond-percolation model, to percolation models in $d>2$ dimensions, and to models with periodic boundary conditions in the perpendicular direction. The detailed reformula-
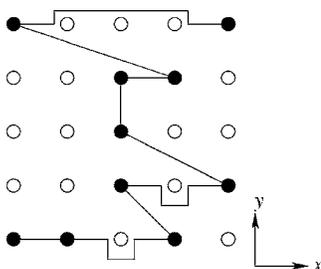

FIG. 4. Illustration of a cluster linkage on a two-dimensional layer of the cylinder $L^2 \times \infty$. The layer is a square lattice with $L = 5$, with periodic boundary conditions in both the x and y directions.
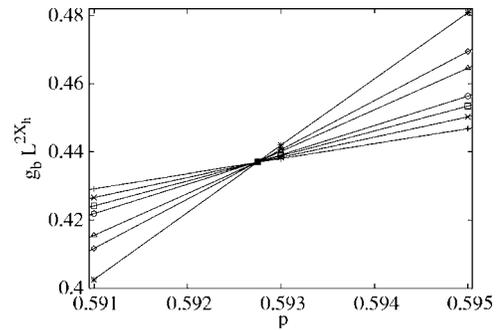

FIG. 5. Scaled magnetic bulk correlation $L^{2X_h} g_b(L/2)$ for the square-lattice site-percolation model vs the site-occupation probability. The bulk magnetic scaling dimension X_h is equal to 5/48. The data points +, ×, □, ○, △, ◇, and ∗ represent system sizes $L=16,24,32,40,64,80$, and 120, respectively.

tion of the algorithm is sufficiently obvious and omitted here, except for one remark about the "linkage" technique for higher dimensions $d>2$. As in two dimensions, we use one number to specify a lattice site in a $(d-1)$-dimensional layer. For instance, for $d=3$, the lattice site (x,y) in the $L \times L$ square layer is labeled by a number $k=(y-1)L+x$. On this basis, one can also arrange the linkage between lattice sites in the same cluster such that it occurs in an increasing order $k_1 < k_2 < \cdots$. An example of such linkages is shown in Fig. 4 for the three-dimensional site percolation model.

We conclude this section by mentioning a property of the linkages for the two-dimensional strip. Consider four sites $k_1 < k_2 < k_3 < k_4$ in a layer. If sites k_1 and k_3 are mutually connected, and so are sites k_2 and k_4, then necessarily all four of them are connected. In other words, no intersections exist between the paths specified by the linkages. The same applies to the layer connectivity of the random-cluster model of the Potts model in two dimensions. This "well-nestedness" property is used in transfer-matrix calculations of the general q-state Potts model. The construction of the transfer matrix requires a one-to-one mapping between allowed connectivities and consecutive integers $1,2,3,\ldots$. The well-nestedness property greatly reduces the number of allowed connectivities.
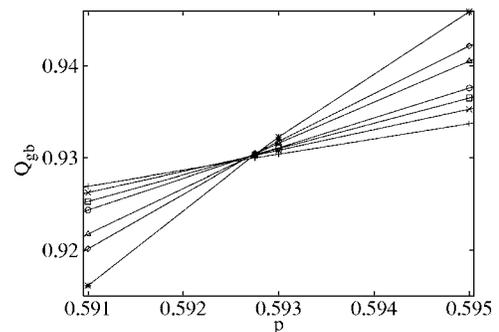

FIG. 6. Bulk ratio Q_{gb} for the square-lattice site-percolation model vs the site-occupation probability. The data points +, ×, □, ○, △, ◇, and ∗ represent system sizes $L=16,24,32,40,64,80$, and 120, respectively.

TABLE I. Summary of percolation thresholds for nearest-neighbor percolation models on the honeycomb, Kagome, square, and triangular lattices. Where exact values are not available, numerical estimates and their references are listed. The parameter z is the coordination number; $p_c^{(b)}$ and $p_c^{(s)}$ represent the critical bond- and site-occupation probabilities, respectively.

	Honeycomb	Kagome	Square	Triangular
z	3	4	4	6
$p_c^{(b)}$	$1-2\sin(\pi/18)$	0.5244053(3) [38]	1/2	$2\sin(\pi/18)$
$p_c^{(s)}$	0.697043(3) [37]	$1-2\sin(\pi/18)$	0.59274621(13) [3]	1/2

III. APPLICATIONS

A. Two dimensions

As mentioned earlier, the nature of phase transition of the percolation model is now well established [7,10–13]. Nevertheless, there still exist critical exponents whose exact values are not available so far, such as the backbone exponent [32–34], and thus numerical studies are needed.

The critical points of several site- and bond-percolation models are also exactly known; for a review, see, e.g., Ref. [35]. These exact results can be obtained [36] by using dual symmetries and matching features of planar lattices, the bond-to-site transformation, and the star-triangle transformation. Table I summarizes some exact percolation thresholds for the honeycomb, Kagome, square, and triangular lattices. The square lattice is self-dual, and the triangular lattice is self-matching. The honeycomb and triangular lattices are dual to each other. However, percolation thresholds of most systems still rely on numerical determinations. The site-occupation percolation thresholds on the honeycomb and square lattices were estimated as $p_c^{(s)}=0.697\,043(3)$ [37] and $p_c^{(s)}=0.592\,746\,21(13)$ [3], respectively, where the superscript (s) specifies the site-occupation probability. The bond-percolation threshold on the Kagome lattice was determined as $p_c^{(b)}=0.524\,405\,3(3)$ [38].

Using the Monte Carlo algorithm developed in Sec. II, we simulate the site-percolation model on an $L\times\infty$ square lattice. Periodic boundary conditions are applied in the perpendicular direction, so that the simulated geometry can be regarded as the surface of a very long cylinder. Initial simulations of $10L$ or more are discarded before sampling procedures are carried out.

As mentioned in Sec. II, the actual simulations were performed on two independent cylinders, and a layer of bulk connectivity is generated after each Monte Carlo step. The sampling procedure thus involves two independent surface layers and one bulk layer. The connectivity of each layer is used to define cluster sizes l_i as the total number of sites in the ith cluster in the present layer. On this basis, the second and fourth moments of cluster sizes are sampled as

$$c_2=\frac{1}{L^2}\sum(l_i)^2 \quad \text{and} \quad c_4=\frac{1}{L^4}\sum(l_i)^4. \tag{1}$$

The parameters l_i, c_2, and c_4, can stand for surface or bulk quantities, and a second index s or b will thus be appended whenever necessary. Then, dimensionless ratios are defined as

$$Q_c=\langle c_2\rangle^2/(3\langle c_2^2\rangle-2\langle c_4\rangle), \tag{2}$$

where the brackets $\langle\rangle$ denote the statistical average. A justification of Eq. (2) can be found in Refs. [39,40].

We also sampled data for the correlation function $g(r)$ on the surface and the bulk layers, defined as the probability that two lattice sites at a distance r are in the same cluster. We chose the distance r as $L/2$ and $L/4$. Accordingly, another dimensionless ratio is defined as $Q_g=g(L/2)/g(L/4)$.

The simulations used 24 system sizes in the range $4\leqslant L\leqslant 20\,000$. For small system sizes, the number of samples was of order $N_s\approx 10^8$ per Monte Carlo run. Note that N_s is the length of the cylinder that is simulated. For $L=20,000$, we took $N_s=4\times 10^6$: taking into account that two cylinders are simultaneously generated, a system of 1.6×10^{11} sites was simulated. For $L=20\,000$, a single run took about 24 hours on a PC running at 700 MHz. The simulations used several independent runs, and the total number of samples per system size was about 1.5×10^9 for $L\leqslant 200$ and 2.0×10^8 for $L>200$.

Parts of the numerical data for the quantities $g_b(L/2)$, Q_{gb}, $g_s(L/2)$, and Q_{gs} are shown in Figs. 5, 6, 7, and 8.

In two dimensions, the consequences of conformal invariance of critical systems have been studied extensively and yielded a large amount of results for both bulk and surface critical phenomena [11,13,41]. A well-known example is Cardy's mapping [42] between the infinite plane (x,y) and the surface of the infinitely long cylinder $(t,k)(1\leqslant k\leqslant L)$. In terms of complex numbers $z=x+iy$ and $w=t+ik$, Cardy's
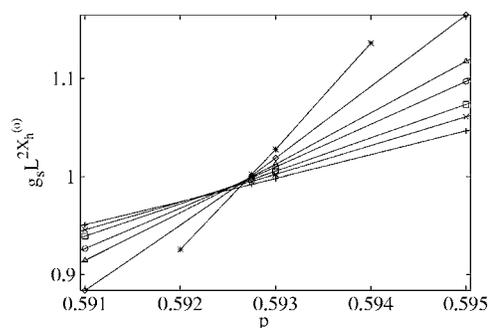

FIG. 7. Scaled surface correlation function $L^{2X_h^{(o)}}g_b(L/2)$ for the square-lattice site-percolation model vs the site-occupation probability. The surface magnetic scaling dimension X_h is equal to 1/3. The data points $+$, $\times$, $\square$, $\bigcirc$, $\triangle$, $\diamond$, and $*$ represent system sizes $L=32,40,48,64,80,120,$ and 200, respectively.

FIG. 8. Surface ratio Q_{gs} for the square-lattice site-percolation model vs the site-occupation probability. The data points $+$, $\times$, $\square$, $\bigcirc$, $\triangle$, $\diamond$, and $*$ represent system sizes $L=32,40,48,64,80,120$, and 200, respectively.

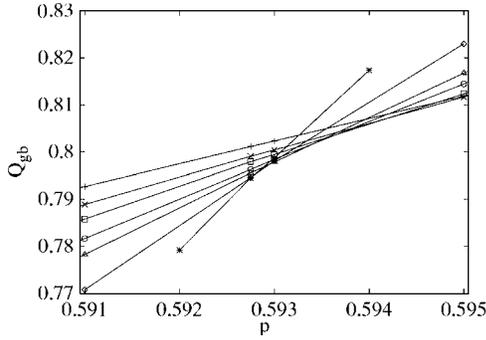mapping reads $w=(L/2\pi)\ln z$. Therefore, the two-point correlation in the (x,y) plane

$$g(x_1,y_1;x_2,y_2) \propto [(x_2-x_1)^2+(y_2-y_1)^2]^{-X} \quad (3)$$

covariantly transforms into

$$g(t_1,k_1;t_2,k_2) \propto \frac{(2\pi/L)^{2X}}{\left[2\cosh\dfrac{2\pi}{L}(t_2-t_1)-2\cos\dfrac{2\pi}{L}(k_2-k_1)\right]^X}, \quad (4)$$

where X can be the bulk thermal and magnetic scaling dimensions, respectively. Equation (4) gives the exact form of two-point correlation functions on the cylinder, apart from an unknown constant factor. On a perpendicular layer, i.e., $t_2=t_1$, Eq. (4) reduces to

$$g(i_1,i_2) \propto \frac{(2\pi/L)^{2X}}{\left[2-2\cos\dfrac{2\pi}{L}(i_2-i_1)\right]^X}, \quad (5)$$

so that one has $g_b(r=L/2)\propto(2\pi/L)^{2X}4^{-X}$ and $g_b(r=L/4) \propto(2\pi/L)^{2X}2^{-X}$. The asymptotic value of the critical bulk
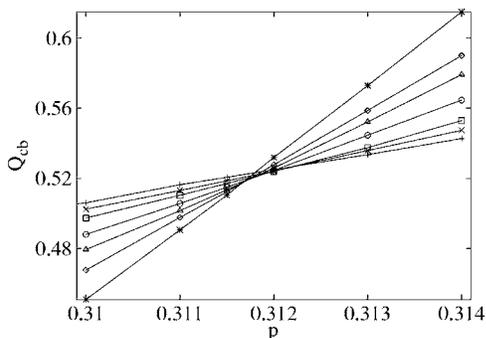

FIG. 9. Bulk ratio Q_{cb} for the simple-cubic site-percolation model vs the site-occupation probability. The data points $+$, $\times$, $\square$, $\bigcirc$, $\triangle$, $\diamond$, and $*$ represent system sizes $L=16,20,24,32,40,48$, and 64, respectively.
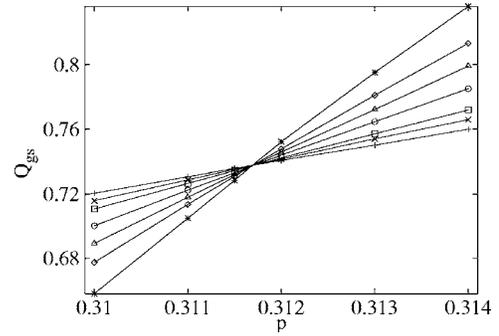

FIG. 10. Surface ratio Q_{gs} for the simple-cubic site-percolation model vs the site-occupation probability. The data points $+$, $\times$, $\square$, $\bigcirc$, $\triangle$, $\diamond$, and $*$ represent system sizes $L=16,20,24,32,40,48$, and 64, respectively.

magnetic ratio $Q_{gb}=g_b(L/2)/g_b(L/4)$ is then equal to 2^{-X_h} $=2^{-5/48}\approx0.930342\cdots$.

Cardy's mapping transforms a semi-infinite plane (x,y) for $y\geq0$ into an infinitely long cylinder with a free surface. Thus, Eq. (5) also holds for surface correlation functions at criticality, and the universal value Q_{gs} is equal to $2^{-X_{hs}^{(o)}}$ $=2^{-1/3}\approx0.793701\cdots$.

In order to estimate the critical probability p_c, we fitted Monte Carlo data for the ratio Q_g and the correlation function g by

$$Q_g(p,L)=Q_{gc}+\sum_{k=1}^{4}q_k(p-p_c)^k L^{ky_t}+b_1L^{y_i}+b_2L^{-2}+b_3L^{-3}$$
$$+b_4L^{-4}+c(p-p_c)L^{y_t+y_i}+n(p-p_c)^2L^{y_t} \quad (6)$$

and

$$g(p,L/2)=L^{-2X}\left(g_0+\sum_{k=1}^{4}g_k(p-p_c)^k L^{ky_t}+b_1L^{y_i}+b_2L^{-2}\right.$$
$$\left.+b_3L^{-3}+b_4L^{-4}+c(p-p_c)L^{y_t+y_i}+n(p-p_c)^2L^{y_t}\right), \quad (7)$$

respectively, where Q_g stands for the bulk and surface ratios Q_{gb} and Q_{gs}, and similar for the correlation function g. Equations (6) and (7) are obtained by Taylor expansions of the finite-size scaling formulas of Q and g. The scaling dimension X in Eq. (7) was fixed at $X_h=5/48$ or $X_{hs}^{(o)}=1/3$ for the bulk and surface correlation functions, respectively. The thermal exponent was fixed at $y_t=3/4$. The correction-to-scaling exponent y_i, arising from the leading irrelevant scaling field, is equal to -2 [11] and -1 [43] for bulk and surface quantities, respectively. The term with coefficient c accounts for the combined effect of the relevant and the leading irrelevant scaling fields, and the term with amplitude n accounts for the nonlinearity of the scaling field as a function of the site-occupation probability $p-p_c$. It can be seen from Figs. 6–8 that Eqs. (6) and (7) satisfactorily describe the general behavior of Q and g: the slopes of the curves increase with L, while the intersections converge to p_c, because all terms in-

dependent of p have negative powers of L. By means of least-squares fits, we obtain $p_c = 0.592\,746\,6(8)$ from Q_{gb}, $p_c = 0.592\,746\,5(4)$ from g_b, $p_c = 0.592\,746\,8(10)$ from Q_{gs}, and $p_c = 0.592\,746\,6(6)$ from g_s. The asymptotic values of the bulk and surface ratios are $Q_{gbc} = 0.930\,34(1)$ and $Q_{gsc} = 0.793\,72(3)$, in agreement with the predictions of conformal invariance, i.e., $Q_{gbc} = 2^{-X_h}$ and $Q_{gsc} = 2^{-X_{hs}^{(o)}}$, as derived above. Fixing Q_{gbc} and Q_{gsc} at the exactly known values leads to essentially the same results and leads only to a small reduction of the estimated statistical errors.

According to the Coulomb gas theory [7,10,12], the second leading bulk magnetic scaling field in the two-dimensional percolation model is also relevant; the associated exponent is $y_{h2} = 2 - X_{h2} = 77/48$. This means that subleading terms with $L^{-X_h - X_{h2}}$ and $L^{-2X_{h2}}$ may exist in bulk magnetic quantities. In terms of corrections to scaling, these can be included in the brackets in Eq. (7) with exponents $y_1 = X_h - X_{h2} = -3/2$ and $y_2 = 2X_h - 2X_{h2} = -3$; the latter has already been included in Eq. (7). Since the bulk ratio Q_{gb} is defined on the basis of g_b, terms with y_1 should also exist in Eq. (6). We therefore also included terms with y_1 in the least-squares analysis of g_b and Q_{gb}, but no substantial evidence was found for such terms.

B. Three dimensions

On the simple-cubic lattice, the critical probabilities for the bond- and site-percolation models are known as $p_c = 0.248\,821\,6(5)$ [44] and $p_c = 0.311\,608\,1(13)$ [39], respectively. The bulk critical exponents were estimated as $y_t = 1.123(25)$ and $y_h = 2.523(4)$ [44,45].

In comparison with two-dimensional systems, phase transitions on the free surfaces of the three-dimensional percolation model appear to display a richer structure. This can be illustrated in the language of the simple-cubic bond-percolation model with bulk and surface bond-occupation probabilities p and $p^{(s)}$. For the "disordered" bulk, i.e., $p < p_c$, the two-dimensional surfaces can sustain long-range order associated with an infinite cluster if the surface parameter $p^{(s)}$ is sufficiently enhanced. A limiting case is bulk probability $p = 0$, in which the surface percolation problem

reduces to the two-dimensional bond-percolation model. Accordingly, a line of "surface" phase transitions $p_c^{(s)}(p)$ occurs. This line $p_c^{(s)}(p)$ meets the bulk critical percolation threshold $p = p_c$ at the "special" phase transition. Depending on the enhancement of $p^{(s)}$, "ordinary" and "extraordinary" surface phase transitions occur at bulk criticality $p = p_c$. The associated surface magnetic exponents were determined [40,46] as $y_{hs}^{(o)} = 1.0246(4)$, $y_{ts}^{(s)} = 0.5387(2)$, $y_{hs}^{(s)} = 1.8014(6)$, and $y_{hs}^{(e)} = 1.25(6)$, where the superscripts (s) and (e) denote the "special" and "extraordinary" transitions, respectively.

Using the Monte Carlo algorithm described in Sec. II, we investigated the site-percolation model on the simple-cubic lattice. The simulations used a geometry $L^2 \times \infty$, with periodic boundary conditions in both of the finite directions. The system size L took 21 values in the range $4 \leq L \leq 1000$. Again, two systems were simultaneously and independently simulated. The length of the transfer direction per system was about 1.0×10^7 for $L \leq 120$, 5.0×10^6 for $200 < L \leq 400$, and 2.0×10^6 for $L > 400$. This means that systems with up to 4.0×10^{12} sites were simulated.

We sampled various bulk and surface quantities, including the moments c_2 and c_4 of the cluster-size distribution, the correlation functions $g(L/2)$ and $g(L/\sqrt{2})$, and the associated dimensionless ratios. The pair correlation function $g(L/2)$ was evaluated over a distance $L/2$ along the x and y directions, and $g(L/\sqrt{2})$ in the diagonal direction of the quadratic layer. Parts of the Monte Carlo data for Q_{cb} in Eq. (2) and for Q_{gs} are shown in Figs. 9 and 10, respectively. The data for Q_{cb}, Q_{gb}, Q_{cs}, and Q_{gs} were fitted by Eq. (6), and those of c_{2b}, g_b, c_{2s}, and g_s by Eq. (7). All the involved critical exponents were left free; these include the bulk thermal exponent y_t and the bulk and surface magnetic dimensions X_h and $X_{hs}^{(o)}$. The correction exponent y_i of the leading irrelevant field was also left free. The results for the above quantities are shown in Table II. In those cases where independent results for the same parameter appear, they are consistent with each other. Next, we simultaneously analyzed the data for Q_{cb}, Q_{gb}, Q_{gs}, c_{2b}, g_b, and g_s, such that the critical exponents and the percolation threshold appear only once in the fitting formulas; for a detailed description of this technique, see Ref. [48]. We
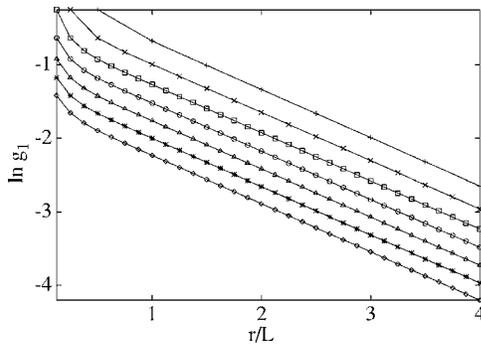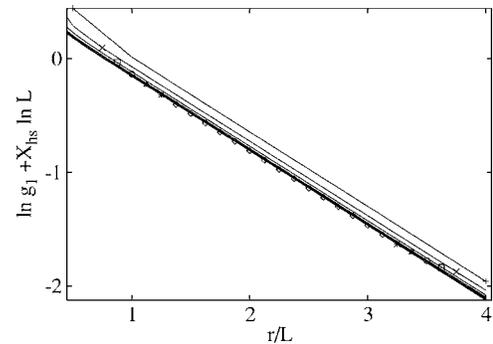

FIG. 11. Logarithm of the order parameter $g_1(r)$ for the square-lattice bond-percolation model at criticality vs the scaled distance r/L to the first layer of the cylinder. The data points $+$, $\times$, $\square$, $\bigcirc$, $\triangle$, $*$, and $\diamond$ represent system sizes $L = 8, 16, 32, 64, 128, 256$, and 512, respectively.

FIG. 12. Logarithm of the order parameter $g_1(r)$ for the square-lattice bond-percolation model at criticality vs the scaled distance r/L. The quantity X_{hs} used to the rescaling of the vertical axis is the surface magnetic dimension at the ordinary phase transition $X_{hs}^{(o)} = 1/3$. The data points $+$, $\times$, $\square$, $\bigcirc$, $\triangle$, $*$, and $\diamond$ represent system sizes $L = 8, 16, 32, 64, 128, 256$, and 512, respectively.

TABLE II. Results of least-squares fits for the site-percolation model on the simple-cubic lattice. The data for sizes $L < L_{min}$ were not included in the fits. The correlation function g was sampled at a distance $L/\sqrt{2}$ in the diagonal direction of the square-lattice layer. The fits of c_{2b}, g_b, and g_s were performed with the thermal exponent y_t fixed at 1.145.

	Q_{cb}	Q_{gb}	Q_{gs}	c_{2b}	g_b	g_s
L_{min}	7	8	8	8	8	8
Q_c	0.5143(2)	0.87299(6)	0.7337(2)			
p_c	0.3116076(4)	0.3116077(6)	0.3116085(18)	0.3116081(6)	0.3116080(4)	0.3116078(9)
y_t	1.1452(8)	1.146(1)	1.144(3)			
y_h				2.5225(2)	2.5226(1)	
$y_{hs}^{(o)}$						1.0247(3)
y_i	−1.5(3)	−2.1(3)		−1.7(3)	−1.8(3)	

obtain $p_c=0.311\ 607\ 7(3)$, $y_t=1.1450(7)$, $y_h=2.5226(1)$, and $y_{hs}^{(o)}=1.0247(3)$. A comparison of our estimates and some existing results is shown in Table III.

We mention that Cardy's mapping in $d>2$ dimensions does not transform the infinite space into geometry $L^{d-1} \times \infty$. Instead, under Cardy's transformation of the space, one obtains the so-called spherocylinder geometry [42,47], which is reached by extending the surface of a d-dimensional sphere into another dimension. Thus, we have no direct relation between the magnetic exponents and the asymptotic values Q_{gbc} and Q_{gsc}.

IV. DISCUSSION

The validity of the algorithm defined in Sec. II is confirmed by the agreement of its results in two dimensions and the predictions of the theory of conformal invariance. The efficiency is reflected by the precision of the three-dimensional results.

The present algorithm has elements in common with those discussed in Sec. I, including the Hoshen-Kopelman routine [16], the transfer-matrix Monte Carlo technique [25], and the Derrida-Vannimenus transfer-matrix approach [27]. Just like the Hoshen-Kopelman method, the simulations are "straightforward," and only a fraction $f<1$ of lattice sites needs to be

stored. In this sense, our algorithm can be regarded as an extension of the Hoshen-Kopelman method. Since the number of clusters is proportional to the volume of the system, the fraction f in the the Hoshen-Kopelman method has a lower bound, i.e., $f>f_0>0$. However, for a d-dimensional percolation model, the present algorithm actually works on $(d-1)$-dimensional layers, and thus f approaches 0 for large system sizes.

In comparison with other cases, the transfer matrix of the percolation model has the special feature that the sum of its elements in each column equals 1. Thus, the matrix can be directly interpreted as a transition probability matrix as used in the transfer-matrix Monte Carlo method. This means that the weight of the random walkers is preserved during the simulation. Population control then becomes unnecessary, and it is sufficient to simulate just one random walker. Therefore, the present method can also be considered as a special case of the transfer-matrix Monte Carlo method [25].

Since systems simulated by our algorithm have an open surface, direct sampling of surface quantities can be performed. Just like the sampling of bulk quantities, the present algorithm is suitable for the study of various types of surface transitions, including the "surface," "ordinary," "special," and "extraordinary" phase transitions. Namely, one may generate an additional layer of percolation configuration with an

TABLE III. Summary of results for site-percolation thresholds on the simple-cubic lattice and the associated scaling exponents.

	Year	p_c	y_t	y_h	$y_{hs}^{(o)}$
Hansen *et al.* [49]	1989				1.04(5)
Grassberger [21]	1992	0.311 604(6)	1.030(6)	2.525(4)	
Lorentz *et al.* [44]	1998		1.12(2)	2.523(4)	
Jan *et al.* [50]	1998	0.311 600(5)		2.530(4)	
Lin *et al.* [45]	1998	0.311 6(1)	1.12(2)	2.49(1)	
Ballesteros *et al.* [39]	1999	0.311 608 1(13)	1.141(2)	2.5230(3)	
Martins *et al.* [51]	2003	0.311 5(3)	1.140(16)		
Deng *et al.* [46]	2003				1.025(4)
Deng *et al.* [40]	2005				1.0246(4)
Present work	2005	0.311 607 7(3)	1.1450(7)	2.5226(1)	1.0247(3)

enhanced surface parameter, and "glue" it on the top of the simulated system.

The conventional way of studying surface critical phenomena is to simulate an L^d lattice with two free surfaces in one direction, as in Ref. [40]. In order to obtain two layers of surface percolation configurations, one then has to produce L layers of configurations. This procedure tends to become computationally expensive, in particular for the "surface" phase transitions, where the bulk is in a "disordered" state. Thus, compared to the conventional simulations, the present algorithm offers a good alternative to study surface transitions.

In Sec. III, the sampling was performed in layers perpendicular to the transfer direction. Nevertheless, it is also possible to keep track of the connectivity along the transfer direction. As an example, we investigated the square-lattice bond-percolation model at its percolation threshold $p_c = 1/2$. The length of the simulated cylinder is four times its circumference, i.e., the transfer dimension was simulated up to a distance $4L$. Fixed boundary conditions were applied to the zeroth layer from which the cylinder starts to grow, and thus all the lattice sites on this layer belong to the same cluster, say cluster 1. Then, the fraction of the lattice sites of the rth layer in cluster 1, $g_1(r)$, was sampled along the transfer direction; the data for $L = 2^3$, 2^4, 2^5, 2^6, 2^7, 2^8, and 2^9 are shown in Fig. 11. Taking into account that the magnetic correlation length along the cylinder is a bulk quantity while the power governing the scaling of $g_1(r,L)$ as a function of L is

the surface magnetic dimension, one has at the percolation threshold

$$g_1(r,L) \propto L^{-X_{hs}^{(o)}} e^{-2\pi X_h r/L}. \tag{8}$$

We mention that, because of the fixed boundary conditions at the first layer of the cylinder, the exponent in Eq. (8) is $X_{hs}^{(o)}$ instead of $2X_{hs}^{(o)}$. For large distance $r \gg 1$, Eq. (8) reduces to $g_1(r,L) = aL^{-X_{hs}^{(o)}} e^{-2\pi X_h r/L}$. This explains why the data lines in Fig. 11 are approximately parallel to each other; the slope is equal to $-2\pi X_h = -5\pi/24$ for $L \to \infty$. Furthermore, the distance between any pair of nearest-neighbor lines in Fig. 11 should be equal to $X_{hs}^{(o)} \ln 2 = (\ln 2)/3$, apart from finite-size corrections. This is confirmed by the rapid convergence of the data lines in Fig. 12, where the vertical axis is $\ln g_1(r,L) + X_{hs}^{(o)} \ln L$.

ACKNOWLEDGMENTS

[1] D. Stauffer and A. Aharony, *Introduction to Percolation Theory* (Taylor and Francis, London, 1992), and references therein.

[2] M. Sahimi, *Applications of Percolation Theory* (Taylor and Francis, London, 1994).

[3] M. E. J. Newman and R. M. Ziff, Phys. Rev. Lett. **85**, 4104 (2000).

[4] P. W. Kasteleyn and C. M. Fortuin, J. Phys. Soc. Jpn. **26** (Suppl.), 11 (1969).

[5] R. B. Potts, Proc. Cambridge Philos. Soc. **48**, 106 (1952).

[6] F. Y. Wu, Rev. Mod. Phys. **54**, 235 (1982).

[7] B. Nienhuis, *Phase Transitions and Critical Phenomena*, edited by C. Domb and J. L. Lebowitz (Academic Press, London, 1987), Vol. 11, p. 1.

[8] J. L. Black and V. J. Emery, Phys. Rev. B **23**, R429 (1981).

[9] M. den Nijs, Phys. Rev. B **27**, 1674 (1983).

[10] B. Nienhuis, A. N. Berker, E. K. Riedel, and M. Schick, Phys. Rev. Lett. **43**, 737 (1979).

[11] J. L. Cardy, *Phase Transitions and Critical Phenomena*, edited by C. Domb and J. L. Lebowitz (Academic Press, London, 1987), Vol. 11, p. 55.

[12] There is a typo in Eq. (4.26) in Ref. [10] for the second-leading magnetic exponent. In this formula, +1 should be replaced by +2.

[13] J. L. Cardy, Nucl. Phys. B: Field Theory Stat. Syst. **240** **[FS12]**, 514 (1984); Nucl. Phys. B **324**, 581 (1989).

[14] G. Toulouse, Nuovo Cimento Soc. Ital. Fis., B **23**, 234 (1974).

[15] R. H. Swendsen and J. S. Wang, Phys. Rev. Lett. **58**, 86 (1987).

[16] J. Hoshen and R. Kopelman, Phys. Rev. B **14**, 3428 (1976).

[17] P. L. Leath, Phys. Rev. B **14**, 5046 (1976).

[18] N. Jan, Physica A **266**, 72 (1999).

[19] P. Grassberger, Phys. Rev. E **67**, 036101 (2003).

[20] R. M. Ziff, P. T. Cummings, and G. Stell, J. Phys. A **17**, 3009 (1984).

[21] P. Grassberger, J. Phys. A **25**, 5867 (1992).

[22] H. W. J. Blöte, J. L. Cardy, and M. P. Nightingale, Phys. Rev. Lett. **56**, 742 (1986).

[23] H. W. J. Blöte, M. P. Nightingale, and B. Derrida, J. Phys. A **14**, L459 (1981).

[24] H. W. J. Blöte and M. P. Nightingale, Physica A **112**, 405 (1981).

[25] M. P. Nightingale and H. W. J. Blöte, Phys. Rev. Lett. **60**, 1562 (1988).

[26] M. P. Nightingale and H. W. J. Blöte, Phys. Rev. B **54**, 1001 (1996).

[27] B. Derrida and J. Vannimenus, J. Phys. A **15**, L557 (1982).

[28] H. J. Herrmann, B. Derrida, and J. Vannimenus, Phys. Rev. B **30**, R4080 (1984).

[29] J.-M. Normand and H. J. Herrmann, Int. J. Mod. Phys. C **6**, 813 (1995).

[30] S. L. A. de Queiroz and R. B. Stinchcombe, Phys. Rev. E **57**, R6245 (1998).

[31] X. Li and D. J. Bergman, J. Stat. Phys. **117**, 427 (2004).

[32] H. J. Herrmann and H. E. Stanley, Phys. Rev. Lett. **53**, 1121 (1984).

[33] P. Grassberger, Physica A **262**, 251 (1999).

[34] Y. Deng, H. W. J. Blöte, and B. Nienhuis, Phys. Rev. E **69**, 026114 (2004).

[35] J. W. Essam, *Phase Transitions and Critical Phenomena*, edited by C. Domb and J. L. Lebowitz (Academic Press, London, 1972), Vol. 2, p. 197.

[36] M. F. Sykes and J. W. Essam, Phys. Rev. Lett. **10**, 3 (1963).

[37] P. N. Suding and R. M. Ziff, Phys. Rev. E **60**, 275 (1999).

[38] R. M. Ziff and P. N. Suding, J. Phys. A **30**, 5351 (1997).

[39] H. G. Ballesteros, L. A. Ferández, V. Martín-Mayor, A. Muñoz Sudupe, G. Parisi, and J. J. Ruiz-Lorenzo J. Phys. A **32**, 1 (1999).

[40] Y. Deng and H. W. J. Blöte, Phys. Rev. E **71**, 016117 (2005).

[41] Y. Deng and H. W. J. Blöte, Phys. Rev. E **67**, 036107 (2003).

[42] J. L. Cardy, J. Phys. A **17**, L385 (1984).

[43] T. W. Burkhardt and J. L. Cardy, J. Phys. A **20**, L233 (1987).

[44] C. D. Lorenz and R. M. Ziff, Phys. Rev. E **57**, 230 (1998).

[45] C. Y. Lin and C. K. Hu, Phys. Rev. E **58**, 1521 (1998).

[46] Y. Deng and H. W. J. Blöte, Phys. Rev. E **69**, 066129 (2004).

[47] J. L. Cardy, J. Phys. A **18**, L757 (1985).

[48] Y. Deng and H. W. J. Blöte, Phys. Rev. E **68**, 036125 (2003).

[49] A. Hansen, P. M. Lam, and S. Roux, J. Phys. A **22**, 2635 (1989).

[50] N. Jan and D. Stauffer, Int. J. Mod. Phys. C **9**, 341 (1998).

[51] P. H. L. Martins and J. A. Plascak, Phys. Rev. E **67**, 046119 (2003).